In Vivo Optical Imaging of Myelination Events in a Myelin Basic Protein Promoter-Driven Luciferase Transgenic Mouse Model

James Cao[1], Yanping Hu[2], Mohammed Salman Shazeeb[1], Carlos E. Pedraza[2], Nilesh Pande[2], Daniel Weinstock[3], Gregory H. Polites[4], Wenfei Zhang[5], Karen J. Chandross[6,*] and Xiaoyou Ying[1,*]

Abstract

The compact myelin sheath is important for axonal function, and its loss can lead to neuronal cell death and irreversible functional deficits. Myelin is vulnerable to a variety of metabolic, toxic, and autoimmune insults. In diseases like multiple sclerosis, there is currently no therapy to stop myelin loss, underscoring the need for neuroprotective and remyelinating therapies. Noninvasive, robust techniques are also needed to confirm the effect of such therapies in animal models. This article describes the generation, characterization, and potential uses for a myelin basic protein-luciferase (MBP-luci) transgenic mouse model, in which the firefly luciferase reporter gene is selectively controlled by the MBP promoter. *In vivo* bioluminescence imaging can be used to visualize and quantify demyelination and remyelination at the transcriptional level, noninvasively, and in real time. Transgenic mice were assessed in the cuprizone-induced model of demyelination, and luciferase activity highly correlated with demyelination and remyelination events as confirmed by both magnetic resonance imaging and postmortem histological analysis. Furthermore, MBP-luci mice demonstrated enhanced luciferase signal and remyelination in the cuprizone model after treatment with a peroxisome proliferator activated receptor-delta selective agonist and quetiapine. Imaging sensitivity was further enhanced by using CycLuc 1, a luciferase substrate, which has greater blood–brain barrier penetration. We demonstrated the utility of MBP-luci model in tracking myelin changes in real time and supporting target and therapeutic validation efforts.

Introduction

Oligodendrocytes, the myelin forming cells of the central nervous system (CNS), belong to a class of glial cells which serve to structurally and functionally support neurons and their axons throughout mammalian life. Upon differentiation, oligodendrocytes become postmitotic and wrap axons in a concentric sheath of compact myelin, which is composed of myelin proteins and lipids. A single mature oligodendrocyte can myelinate up to 50 axons, with each extension contributing to an internode segment along the continuum of that axon (Raff &

[1]Translational In Vivo Model, Global Research Platform, Sanofi R&D, Framingham, MA, USA
[2]Multiple Sclerosis Cluster, Neuroscience Research, Sanofi R&D, Framingham, MA, USA
[3]Janssen Research and Development, Spring House, PA, USA
[4]Regeneron Pharmaceuticals, Tarrytown, NY, USA
[5]Biostatistics and Programming, Sanofi R&D, Framingham, MA, USA
[6]Strategic Initiatives and Science Relations, Bridgewater, NJ, USA
*These authors contributed equally as co-senior authors to the original concept and development of the MBP-luci model.

Corresponding Author:
James Cao, Principle Investigator, Translational In Vivo Model, Global Research Platform, Sanofi R&D, 49 New York Avenue, Framingham, MA 01701, USA.
Email: james.cao@sanofi.com

Lillien, 1988; Barres & Raff, 1999; Nakahara et al., 2009; Piaton et al., 2009; Corboy & Miravalle, 2010; Zhang et al., 2012; Grade et al., 2013).

Multiple sclerosis (MS), a demyelinating disease of the CNS, is one of the primary causes of neurological disability in young adults, and the loss of myelin forming oligodendrocytes at lesions is thought to be a primary contributor to its pathophysiology. Oligodendrocyte progenitor cells (OPCs), which are present throughout life, can migrate to regions of injury and replace lost myelin, including in MS lesions (Adams, 1989; Chang et al., 2000; Decker et al., 2001). There is evidence for successful remyelination in MS lesions. However, this process appears to be inefficient and eventually succumbs to the effects of negative regulators of repair, repeated insult, and age, thereby creating a niche for drug therapies that can overcome these barriers. In this way, myelin repair processes can be driven effectively to protect neurons that would otherwise die (Plemel et al., 2017). Toward this end, noninvasive techniques are needed to quantitatively assess therapeutic effects in animal models over time and thereby support the development of neuroprotective and remyelinating therapies.

CNS myelin is synthesized by differentiated oligodendrocytes and is composed of various lipids and myelin proteins, including myelin basic protein (MBP), proteolipid protein (PLP), and myelin oligodendrocyte glycoprotein (MOG; Jurevics et al., 2002). During OPC differentiation, myelin constituents are expressed sequentially, starting with galactosylceramide and followed by MBP, PLP, and MOG. MBP, which is located within lipid bilayers, is required for normal myelin compaction around individual axons and, as such, represents a marker of oligodendrocyte maturation (Miron et al., 2011). The MBP promoter contains four widely spaced conserved regulatory elements, M1, M2, M3, and M4, ranging from 0.1 to 0.4 kilobase (kb), which are critical for regulating the timing of myelination and remyelination events (Farhadi et al., 2003). In the CNS, the proximal modules M1 and M2 drive relatively low-level expression in OPCs during CNS development, whereas the upstream M3 region drives high-level expression in oligodendrocytes throughout development and in the adult CNS. Moreover, the M3 region is required for myelin expression during remyelination after a demyelinating insult.

In this article, we describe the generation, characterization, optimization, and application of a new transgenic mouse model that uses the MBP promoter region, spanning M1 through M4, to selectively drive expression of firefly luciferase (MBP-luci) in myelin forming glial cells. This transgenic model, when used in conjunction with established bioluminescence imaging (BLI) techniques, offers a powerful tool for following gene expression changes. MBP-luci line 171 (spanning the M1–M3 promoter region of MBP) was used to selectively track oligodendrocyte demyelination and remyelination events longitudinally in the CNS of living mice. This line was also used to assess the effect of brain penetrable small molecules on remyelination and myelin protection in the cuprizone lesion model of demyelination after therapeutic treatment (initiated after removal of cuprizone diet) with a Sanofi peroxisome proliferator activated receptor-delta (PPAR-δ) selective agonist (S711) or prophylactic treatment (initiated at the start of cuprizone diet) with the serotonin or dopamine receptor modulator, quietiapine (QTP). Finally, signal detection was further enhanced by using the blood–brain barrier penetrable luciferase substrate, CycLuc 1, in albino mice to improve imaging sensitivity without the removal of fur.

Materials and Methods

Generation of MBP-Luci Transgenic Mice

Either pGL3-hygro-MBP10k-luci or pGL3-hygro-MBP5k-luci plasmids (Supplemental Figure 1) were digested with NotI and BamH1 enzymes. A fragment containing the MBP promoter luciferase and polyadenylation signal was then gel purified. Transgenic mice were generated by standard pronuclear injection into cell embryos from FVB, B6C3H, or C57BL/6 (Jackson Lab) following published protocols (Polites & Pinkert, 2002).

Transgenic-positive founder mice and their transgenic positive G1 offspring were identified by polymerase chain reaction (PCR) of tail biopsy DNA using primers specific for the firefly luciferase gene (PCR primers: 5′gaa atgtccgttcggttggcagaagc-3′ and 5′ccaaaaccgtgatggaat ggaacaaca-3′). All animal work was performed in accordance with federal guidelines. Three different strains of mice (FVB, B6C3H, and C57BL/6) were used (Figure 1(a)).

BLI in MBP-Luci Transgenic Mice

Experimental protocols were approved by Sanofi's institutional animal care and use committee, and studies were conducted in Sanofi's association for assessment and accreditation of laboratory animal care accredited facility. Whole-animal bioimaging was conducted with the IVIS in vivo imaging system (Xenogen IVIS-100, IVIS-lumina, or IVIS spectrum, PerkinElmer, Hopkinton, MA) to screen MBP-luci lines and compare imaging signals. Unless otherwise stated, one day before imaging, mouse head fur (between the ears, nose to neck region) was removed with cream (Nair, Church & Dwight Co., Inc., Ewing, NJ) and rinsed. Mice were anesthetized with isoflurane and injected subcutaneously with 200 mg/kg D-luciferin salt (PerkinElmer, Hopkinton, MA) or 15 mg/kg CycLuc 1 sodium salt (Aobious, Gloucester,
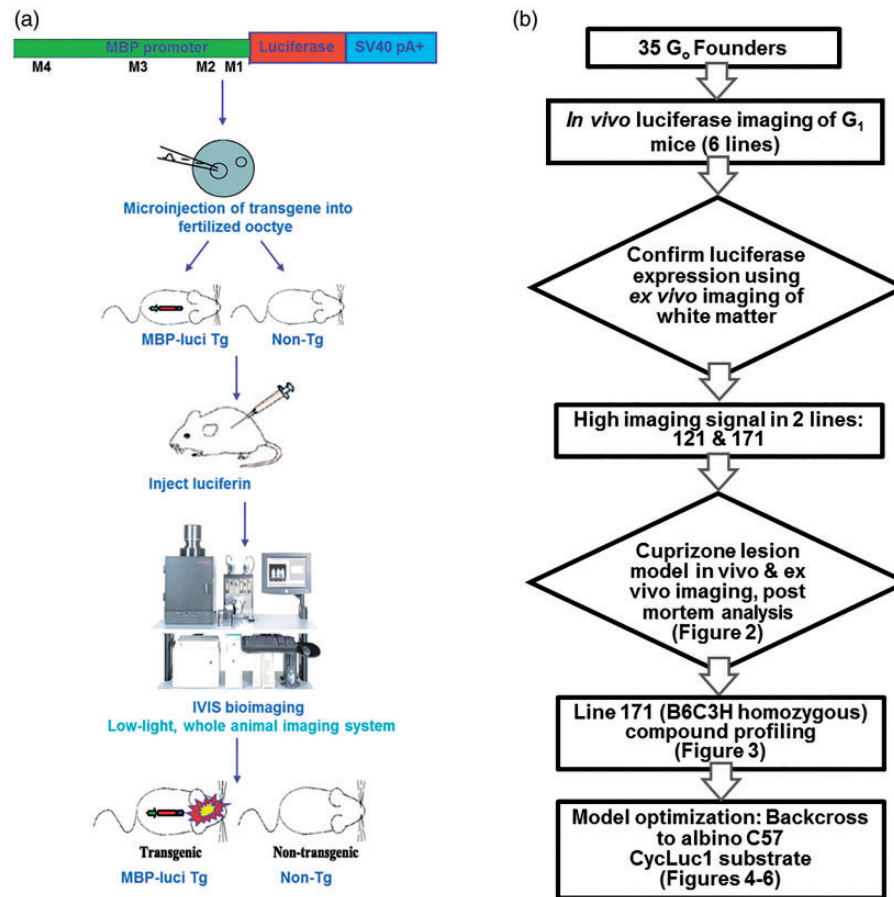
Figure 1. MBP-luci transgenic line generation and validation steps. (a) MBP-luci transgene utilized endogenous promoter control elements that regulate expression in oligodendrocytes. M1 to M3 (5 kb) or M1 to M4 (10 kb) promoter regions were cloned from a BAC library and then inserted into a firefly luciferase expression vector. MBP promoter-driven luciferase expression cassettes were micro-injected into fertilized FVB or B63CH oocytes at the single cell stage to generate transgenic founder mice. (b) Thirty-five founder lines were identified via PCR. Six lines demonstrated detectable luminescence signal upon subcutaneous injection of luciferin (Supplemental Figure 2), and two lines demonstrated superior signal intensity, as assessed by *in vivo* and ex vivo imaging: Lines 171 (Figure 2) and 121 (Supplemental Figure 3). Line 171 was then bred to homozygosity and tested in the cuprizone model of de/remyelination (Figure 3). MBP-luci model signal detection was further enhanced by backcrossing to albino C57BL/6 and using the CycLuc1 substrate (Figures 4–6).

MA) dissolved in phosphate-buffered saline without calcium chloride and magnesium chloride. Eight minutes after the substrate injection, mice were placed in the IVIS imaging chamber stage (maintained at 37°C) and imaged with 1 min exposure every 2 min up to 25 min. Different substrate concentrations, dosing routes, imaging exposure times, and other imaging parameters were optimized for the maximum and consistent bioluminescence signal. Imaging kinetic curves were obtained for each mouse, and peak imaging value was selected. Usually five mice were imaged per group. The field of imaging was set to cover five mice and the medium binning, and the f-stop 1 or 2 was used. A pseudo color scheme (generated by the living imaging$^{@}$ software, Xenogen or PerkinElmer) was used to visualize the numerical contents of the acquired bioluminescent signal (superimposed onto contrast, gray-scale

photographic pictures to determine the bioluminescence signal location). To quantify bioluminescence emission signal, identical regions of interest (ROI) were positioned to encircle each mouse head region, the imaging signal was quantitated as average radiance (photons/s/cm^2/ steradian), and the imaging signal graphic output was listed as photon flux (photons/s) for the indicated ROI. As long as the ROI is kept constant in area and position for a study, these two units are proportional. Data were normalized to bioluminescence prior to the initiation of treatment for each animal.

Ex vivo BLI of isolated organs was performed immediately after euthanasia of the animals by CO_2, 10 min after subcutaneous injection of luciferin (200 mg/kg). Dissected organs were placed on a black paper covered with plastic sheet and imaged. Bioluminescent signals usually remained detectable within 10 to 20 min after dissection.

Tissue Preparation and Histological Staining

At indicated time points, animals were euthanized with CO_2 and perfused with phosphate-buffered saline via the left cardiac ventricle. The brains were dissected, fixed in 10% neutral formalin for 48 hr, and then transferred into 70% ethanol for embedding, sectioning, and staining. Brains were sectioned coronally between bregma 0.74 and bregma 1.0. Then 5-µm serial paraffin sections were made such that each slide had two sections with 30 µm difference between the two sections to capture the corpus callosum at different levels.

Sections were deparaffinized, stained with luxol fast blue (LFB), and counterstained with nuclear fast red. Slides were scanned using a Leica scanner (Aperio XT, Buffalo Grove, IL). Images from at least eight sections were collected, and quantitative image analysis was performed using Definiens Tissue Studio software (Definiens, Munich, Germany).

Cuprizone Mouse Model of Demyelination and Remyelination

The cuprizone lesion model was used as described earlier (Jurevics et al., 2002; Miron et al., 2011) to induce demyelination and follow remyelination events in the corpus callosum region enriched with oligodendrocytes. In all studies, 8- to 10-week-old female and male homozygous MBP-luci transgenic mice were used unless otherwise specified. Demyelination was induced by feeding a diet containing 0.2% cuprizone (bis-cyclohexanone oxaldihydrazone; Sigma-Aldrich Inc., St. Louis, MO) for 4 or 5 weeks. Thereafter, mice were fed a normal powder diet for another week for remyelination studies. The 0.2% cuprizone diet was freshly mixed with grounded powder of normal rodent chow. The control mice also received freshly grounded powder of normal rodent chow. The cuprizone or normal diet was changed twice per week. Food and water were available ad libitum, and mice were weighed weekly.

Compound Profiling

MBP-luci B6C3H line 171 (both heterozygous and homozygous) was used to assess the effect of small molecule modulators of two distinct signaling pathways: PPAR-δ agonist (S711) and the well-characterized serotonin or dopamine receptor antagonist QTP.

For the PPAR-δ agonist study, 8-week-old homozygous mice ($n = 12$ per group) were placed on a diet containing 0.2% cuprizone for 26 days and then given normal diet to allow for endogenous remyelination. After removal of the cuprizone diet, mice were orally dosed, twice daily, with either vehicle (0.6% carboxymethylcellulose sodium salt and 0.5% Tween 80) or S711 (30 mg/kg; designed and synthesized at Sanofi) for

8 days and imaged at different time points. Data were normalized to pretreatment (Week 0) baseline signals.

For the QTP study, 8-week-old homozygous mice were placed on a diet containing 0.2% cuprizone and in parallel, orally dosed, once daily, with vehicle (water) or QTP (10 mg/kg) for 5 weeks and imaged weekly. For both PPAR-δ and QTP studies, the same experimental design was performed with line 171 heterozygous mice and generated similar results (data not shown).

Magnetic Resonance Imaging

Magnetic resonance imaging (MRI) measurements for the cuprizone model were performed at the 4-week time point using a 7T preclinical MRI scanner (Biospin, Bruker, Billerica, MA) with a 72-mm volume coil (Bruker, Billerica, MA) and a 10-mm quadrature surface coil (Bruker, Billerca, MA) served as the receiver. Multislice multi-echo T2-weighted (T2W) images were acquired using a rapid acquisition with relaxation enhancement sequence (TR/TE = 2500 ms/10 ms, 8 echoes, echo spacing = 10 ms, number of excitations = 2), and T2 maps were calculated using a single exponential decay. To calculate magnetization transfer (MT) ratio (MTR) maps, fast low angle shot (FLASH) images (TR/TE = 70 ms/6 ms, 10° flip angle, number of excitations = 48) were acquired both with and without an MT saturation pulse (Gaussian shaped, 10.25 ms long, 10 µT peak power, 6 kHz offset). MTR and T2W images were acquired with 0.75-mm slice thickness (six coronal slices), 25-mm field-of-view, and matrix size of 256×256. For data analysis, an ROI was drawn around the visible corpus callosum structure across the six coronal slices in the MTR maps to calculate the corpus callosum area and the MTR values. The same ROIs were overlaid on the T2 maps to calculate the T2 values. The individual slices from each animal were grouped together for statistical comparisons between the two groups.

Statistical Analysis

Each of the measurements in Figures 2(c), 5(c), and 6 is compared between two treatment groups using two-sample t tests. For the comparison of BLI signals (Figure 4(b)) in the brain and intestines for two types of substrates, two-sample t tests were performed at each of the study time points and corrected for multiple comparisons using the Holm-Sidak method. A two-way analysis of variance model was applied to the data in Figures 3 and 5(a) with random effect nested in mouse, using treatment, time (categorized), and their interactions as covariates. The comparisons among different treatment groups at each time point was evaluated with p value adjusted by Holm–Bonferroni method. For the
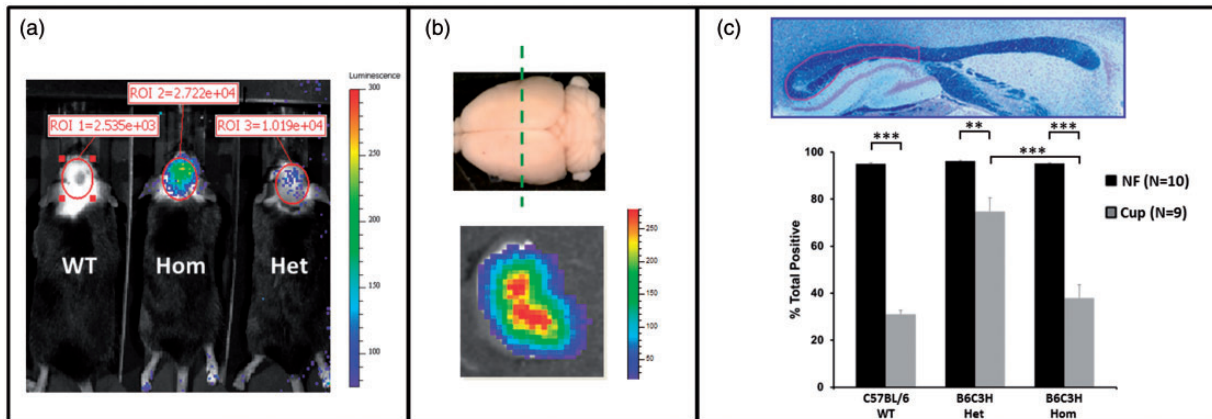
Figure 2. MBP-luci line 171 B6C3H validation. (a) *In vivo* imaging of a representative wild-type B6C3H mouse (WT; no transgene; left side of panel) showing background bioluminescence in the cranium region of interest (ROI) that measured 2.5×10^3 photon counts per second (photons/s). A representative heterozygous MBP-luci mouse (right side of panel) measured bioluminescence in the ROI at 1.0×10^4 photons/s and homozygous MBP-luci mouse (center panel) measured at 2.7×10^4 photons/s with homozygous mice showing >twofold increase in the signal intensity as compared with heterozygotes. Similar results were seen in >100 mice, and this method was used to confirm homozygosity. (b) Serial coronal sections of whole brains assessed ex vivo for brain subregion transgene activity showed strongest bioluminescence (red and yellow pixels) in the corpus callosum, a region enriched with oligodendrocytes. (c) LFB densitometry was performed on sagittal sections of the corpus callosum. Homozygous mice showed comparable demyelination as wild-type C57BL/6 mice (similar decrease in % total positive) after 4 weeks on the cuprizone diet ($\sim$60% decrease in % total positive), as determined by quantitative morphometric analysis. Heterozygous mice were more resistant to the cuprizone diet ($\sim$20% decrease in % total positive). Statistically significant differences using two-tailed *t* test analysis are indicated on the plot.

correlation between BLI at each time point and each of the histology and MRI parameters, Spearman's rank correlation coefficient method was used (Figure 5(e) and Supplemental Table 2). Significance is indicated in the figures by asterisks (*.01 < p < .05, **.001 < p < .01, ***p < .001). All two-sample *t* tests were performed with GraphPad Prism software (GraphPad Software, Inc., La Jolla, CA). All other analysis was performed with R version 3.4.1.

Data and Transgenic Model Availability

All MBP-luci transgenic lines are listed in the Supplemental Table 1. These transgenic lines request should be addressed to FRASA-MailBox@sanofi.com. The experimental data sets that were generated or analyzed in the current article are available from the corresponding authors on reasonable request.

Results

Generation of MBP-Luci Mouse Lines and Analysis of Differential Expression

To study myelin dynamics *in vivo* by means of a noninvasive method, we established mouse MBP reporter lines. MBP promoter elements M1 through M4 have been described to regulate different aspects of OPC

differentiation, myelin synthesis, and structure (Farhadi et al., 2003). Upon cloning of M1 to M3 or M1 to M4 promoters from the BAC library, a 5 kb or 10 kb promoter was inserted into a firefly luciferase expression vector. Then MBP promoter-driven luciferase expression cassettes were used for microinjection into fertilized oocytes to generate transgenic founder mice, as described in Material and Methods section, and 35 founders were identified by means of PCR (Figure 1(a)). Out of these, six lines showed positive luminescence signal upon subcutaneous injection of luciferin, and two lines were selected for their high signal intensity when analyzed ex vivo in brain white matter sections. Lines labeled as 121 (MBP promoter M1–M4) and 171 (MBP promoter M1–M3) were further analyzed in studies with the cuprizone animal model of de/remyelination. Based on robust reporter gene expression, line 171 was then selected for the remainder of studies described in this report. Following several trial iterations for luciferin dosing and imaging optimization, line 171 was backcrossed to the albino C57BL/6 strain for additional experimentation including MRI imaging validation (Figure 1(b)).

As expected, homozygous mice from the founder B6C3H line 171 showed over twofold stronger luminescence signal as compared with heterozygous mice (Figure 2(a)) and were used for subsequent studies, including backcrossing into a C57BL/6 albino strain. As illustrated in Figure 2(b; coronal section of
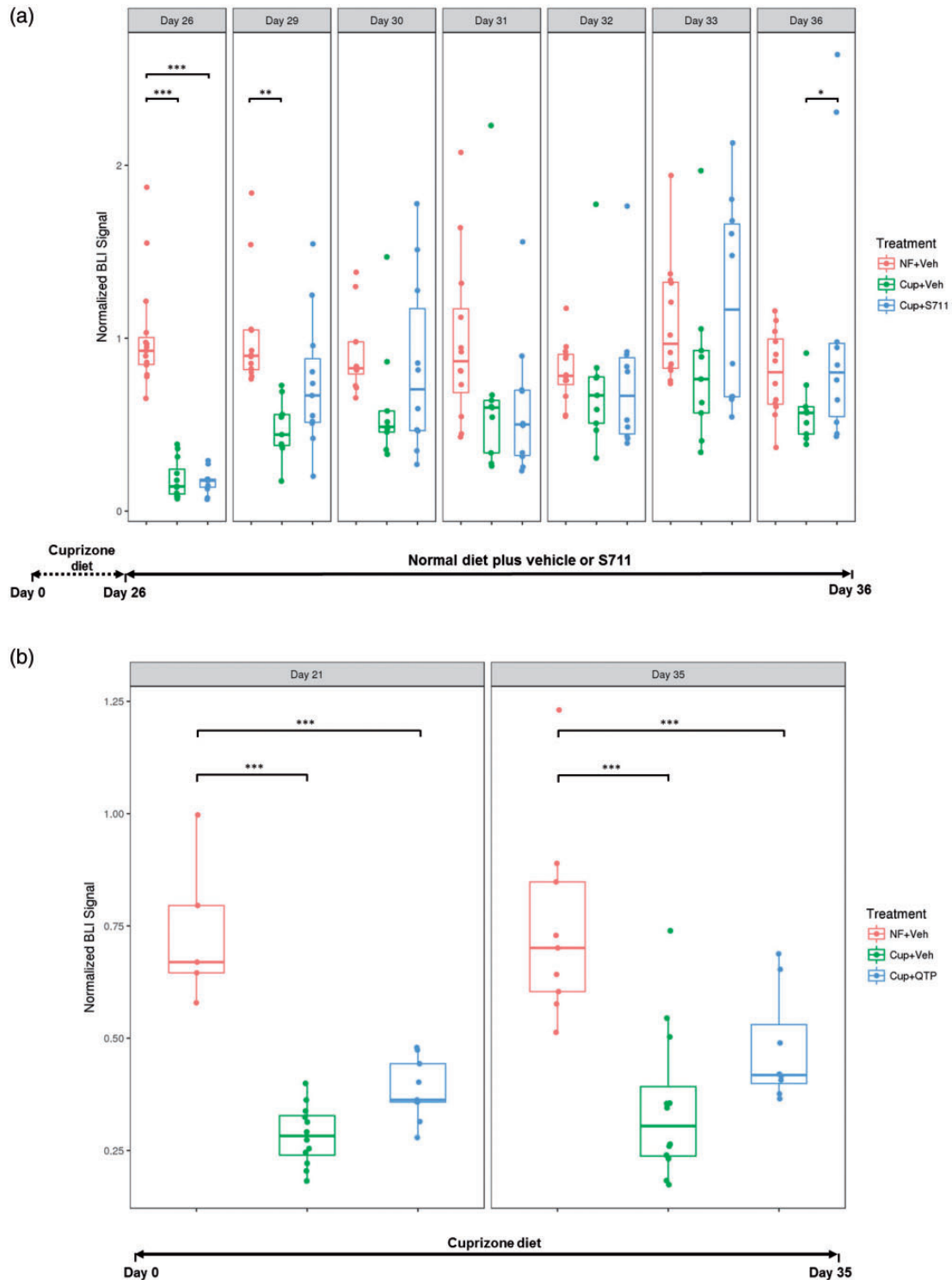
Figure 3. A PPAR-δ agonist, S711, and QTP separately enhanced luciferase activity in the cuprizone model. (a) Eight-week-old MBP-luci mice (line 171, homozygous, B6C3H strain; Day 0) were placed on a 0.2% cuprizone diet for 4 weeks to cause demyelination, which resulted in an 80% decrease in relative luciferase imaging signal at Day 26 compared with the normal food (NF) group. On Day 26, the normal food diet was resumed to allow for spontaneous remyelination, and mice were dosed orally, twice daily, with vehicle (0.6% carboxymethylcellulose sodium salt and 0.5% Tween 80) or S711 (30 mg/kg) for 8 days and imaged at the indicated time points. At Day 36, relative luciferase signal increased for the cuprizone group treated with S711 (Cup + S711) as compared with the cuprizone group treated with vehicle (Cup + Veh; two-way analysis of variance model with multiple measurement adjustment $*p = .015$). (b) At Day 0, homozygous MBP-luci mice were fed a diet of 0.2% cuprizone for 5 weeks and, in parallel, dosed orally, once daily, with QTP (10 mg/kg; Cup + QTP) or vehicle (Cup + Veh). There is a trend of QTP (Cup + QTP) protection against cuprizone-induced loss of luciferase signal compared with the vehicle group (Cup + Veh; two-way analysis of variance model with multiple measurement adjustment, $p = .15$ for Day 21 and $p = .61$ for Day 35). Data were normalized to Day 0 baseline signals for each mouse.
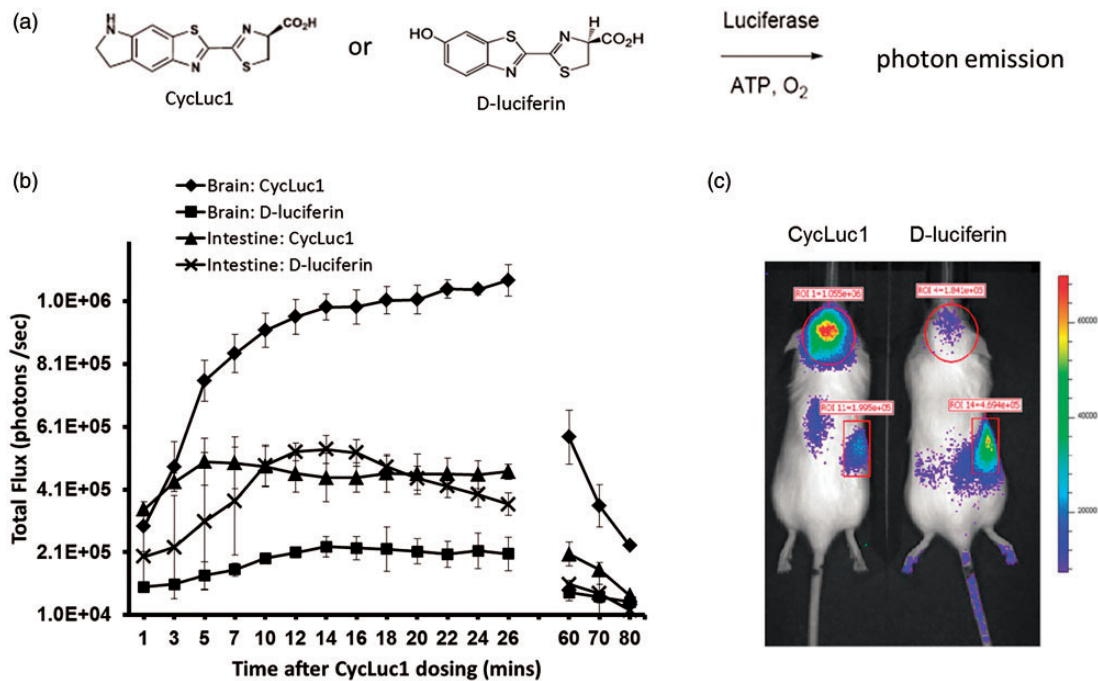
Figure 4. MBP-luci model optimization: The MBP-luci line 171 B6C3H mice were backcrossed onto the C57BL/6 albino strain to improve luciferase signal detection. (a) Cartoon depicting the bioluminescence reaction for CycLuc1 or D-luciferin substrates. (b) Comparison of CycLuc1 (15 mg/kg) and D-luciferin (200 mg/kg) substrate imaging with albino C57BL/6 MBP-luci homozygous mice ($n = 3$ per group) without shaving. In the brain, CycLuc1 showed approximately a fivefold increase in signal intensity compared with D-luciferin over a 26-min period (multiple t test showed statistically significant difference between the 3-min and 60-min time window with p value ranging from $.0001 < p < .01$). D-luciferin initially showed approximately a twofold signal increase compared with CycLuc1 in the intestines (multiple t test showed statistically significant difference at the 1- and 3-min time points with p values from $.001 < p < .01$) but the levels evened out by 5 min (no significant difference). For all groups, by 80 min, the signal intensity rapidly decreased. (c) Representative image from the 20-min time point showed approximately a fivefold increase in signal intensity in the brain with CycLuc1 compared with D-luciferin. D-luciferin showed approximately a twofold signal increase compared with CycLuc1 in the intestines.

homozygous mouse), in the adult mouse brain, the highest luciferase signal intensity corresponded to deep white matter tracts which are enriched with myelin lipids and myelin proteins. Line 121 (FVS strain) *in vivo* and ex vivo imaging also confirmed that the corpus callosum region in the brain had the highest bioluminescence signal (Supplemental Figure 3).

During demyelination, such as that caused by the consumption of cuprizone, a copper chelator mixed in the diet, a decrease in luciferase signaling was predicted. Although in wild-type C57BL/6 mice, cuprizone-mediated demyelination is easily detectable in areas of high myelin content, including the corpus callosum (Lindner et al., 2008; Mangiardi et al., 2011), strain differences have been reported, including findings that certain strains do not respond to cuprizone as well as the most extensively characterized C57BL/6 strain (Elsworth & Howell, 1973; Yu et al., 2017). Because no brain imaging positive transgenic C57BL/6 strain founder could be generated, the B6C3H strain line 171 had to be tested for suitability for use in cuprizone-mediated demyelination experiments. Line 171 was responsive to detecting

myelin changes in the cuprizone model showing levels of demyelination in the corpus callosum (sagittal section) comparable to that detected in C57BL/6 strain (30–60% demyelination), as determined by densitometry of LFB staining on sagittal sections of the corpus callosum (Figure 2(c)). Demyelination in homozygous B6C3H line 171 was significantly higher than in heterozygous mice of the same strain and comparable to wild-type C57BL/6 mice. As such, homozygous B6C3H line 171 mice were used for all subsequent studies, including backcrossing into a C57BL/6 albino strain for MRI imaging studies.

Longitudinal, Noninvasive Tracking of Myelin Changes During Demyelination and Remyelination Using the MBP-Luci Mice

MBP-luci line 171 was assessed for the ability to detect changes in myelin content *in vivo* upon demyelination and remyelination in the cuprizone model, based on the intensity of luciferase signal. In addition, the effect on remyelination and protection of myelin was assessed in
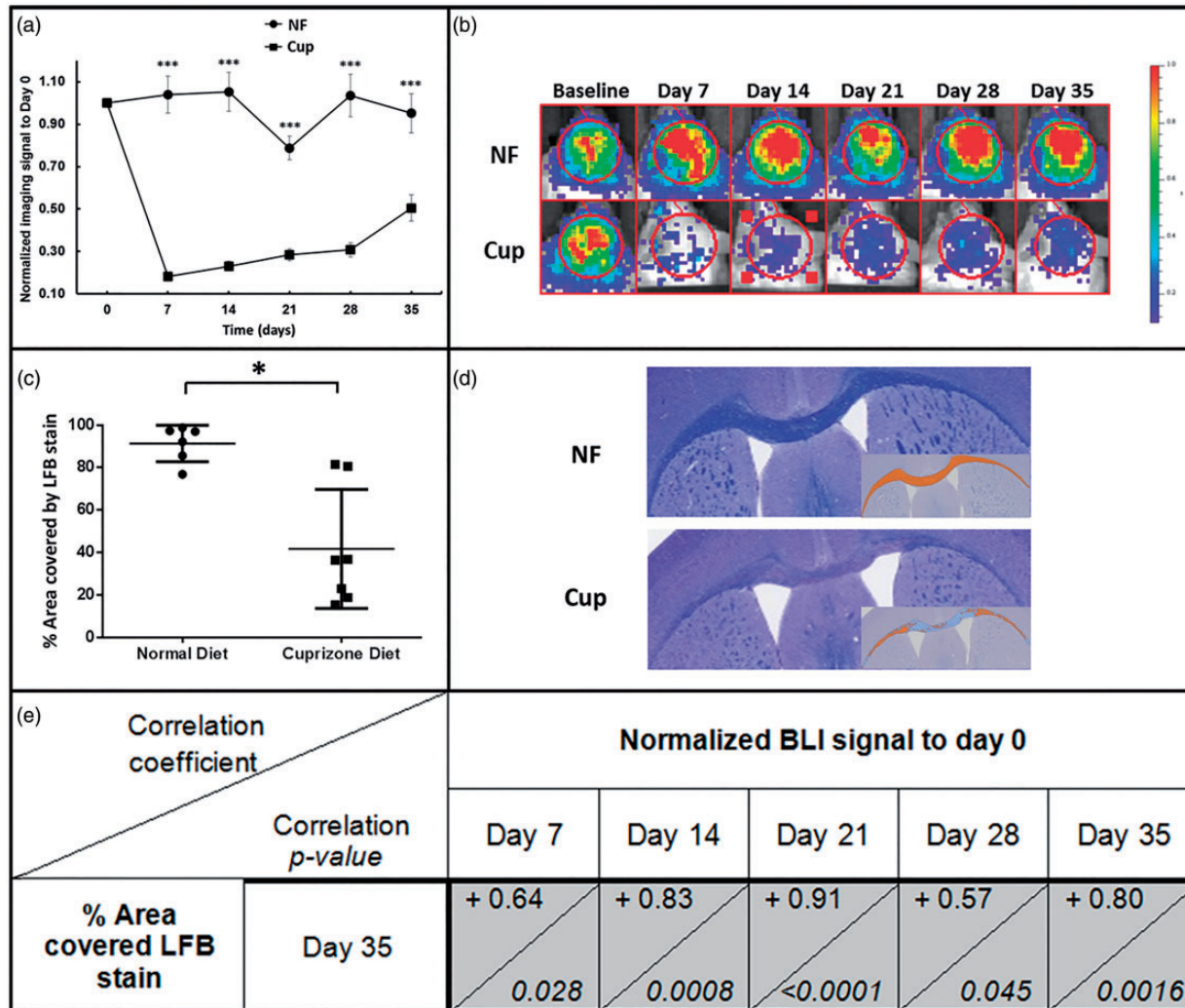
Figure 5. C57BL/6 Albino MBP-luci mice line utility in the cuprizone model. Mice were maintained on a 0.2% cuprizone diet for 35 days. (a) Luciferase bioimaging signal is shown for the normal food (NF, $n = 12$) and cuprizone (Cup, $n = 12$) diet groups up to 35 days. There was a significant decrease in luciferase activity in the brain after 7 days on the cuprizone diet ($\sim$80% reduction), similar to line B6C3H. Two-way analysis of variance showed a statistically significant difference between NF and Cup groups for all time points after Day 0 (***$p < .0001$). A trend toward increasing luciferase signal intensity occurred after Day 7. Imaging signal was normalized to Day 0. (b) Representative brain images of live mice (without shaving head) on a normal food (NF) or cuprizone (Cup) diet tracked longitudinally from Day 0 (baseline) through Day 35 and demonstrating reduced signal intensity on the cuprizone diet. (c) LFB staining at Day 35 confirmed demyelination in the cuprizone diet group ($n = 7$) showing a significant difference compared with normal diet group ($n = 6$) between the two groups using t test (*.01 < p < .05). (d) Representative images of LFB stained coronal sections counterstained with NFR (insets) at Day 35 confirming demyelination in the corpus callosum of cuprizone-fed (Cup) mice. (e) Correlation analysis of bioluminescence imaging (BLI) signal (at Day 7, 14, 21, 28, and 35) with histology LFB staining (at Day 35) are shown. The Spearman correlation coefficient and corresponding p values are indicated in the shaded boxes.

this model using two pharmacological agents that modulate signaling pathways known to affect oligodendrocyte maturation and myelination, namely a PPAR-δ selective agonist, S711, and the serotonin or dopamine receptor modulator, QTP (Iwashita et al., 2007; Zhang et al., 2012).

Homozygous mice were fed a cuprizone diet (0.2% in chow) for 26 days to induce demyelination, and bioluminescence signal was measured in comparison to animals on a normal diet (Figure 3(a)). A significant reduction in luciferase activity was observed in mice on the cuprizone diet during the demyelination phase (Day 0–Day 26), which was attenuated with S711 treatment by Day 29 (30 mg/kg, twice daily for 8 days) when compared with vehicle. S711 treatment group had a greater variance compared with vehicle group for all days up to Day 36. S711 treatment effect was statistically significant at the last time point Day 36 ($p = .0153$, S711 vs. veh). This

same PPAR-δ agonist S711 stimulated MBP protein expression after 7 days exposure to cultured rat OPCs in a concentration dependent manner (novel finding; Supplemental Figure 4).

In addition, administration of QTP (10 mg/kg, once daily), shown to protect and induce OPC maturation in rodents (Bi et al., 2012), prevented cuprizone-induced demyelination, as indicated by an increasing luciferase signal trend at Day 21 and Day 35 shown in Figure 3(b).

Optimization of Luciferase Signal in C57BL/6 Albino Strain and Measurement of Demyelination in the Cuprizone Model

Upon confirmation of the utility of the MBP-luci mouse for measuring changes in myelin content and as a part of the model optimization, the B6CH3 line was back-crossed onto the C57BL/6 albino strain for homozygous on Tyr^{c-2J}. Their skin, hair, and eye color are the same as the albino strain (no pigment), so we could avoid black fur signal interference and the need for shaving before imaging. Also, a different luciferase substrate, CycLuc1 sodium salt (Evans et al., 2014) was compared with D-luciferin for signal strength. As shown in Figure 4, CycLuc1 required much lower doses than D-luciferin (15 mg/kg vs. 200 mg/kg) because of its superior brain and cellular penetrability (Adams & Miller, 2014). CycLuc1 resulted in a significantly stronger signal in the brain, which was detected in less than 5 min after administration and was maintained at high levels after 15 min, reaching approximately five times the intensity of D-luciferin at 20 min post injection (Figure 4(b)). Multiple t test showed statistically significant difference $(.0001 < p < .01)$ between the 3 min and 60 min time window.

For line 171 mice, in addition to the brain, luciferase signal was also detected in the intestines (Figure 4), and the signal was stronger using D-luciferase as compared with CycLuc1 as a substrate. These findings suggest differential substrate bioprocessing, tissue distribution, or metabolic elimination. Consequently, biodistribution and cellular uptake differences can have a significant impact on signal intensity as demonstrated previously with radioiodine labeled D-luciferin (Lee et al., 2003) and 14C-D-luciferin pharmacokinetic studies, which detected limited substrate concentrations in the brain, bone, and muscle (Berger et al., 2008). Signal decay was detected after 70 min of dosing reaching baseline levels by 100 min (Figure 4(b)).

We next tested the stronger signal detected with CycLuc1 in the MBP-luci C57BL/6 albino mouse line in demyelination conditions in the cuprizone model. There was a dramatic decrease in luciferase activity in the brain of curpizone-demyelinated mice by Day 7, which was maintained at low levels after 28 days on the cuprizone diet $(p < .0001$ for all time points) and showed

a trend toward recovery by 35 days (Figure 5(a) and (b)). Cuprizone-fed mice showed demyelination in the corpus callosum as determined by LFB staining and quantification by densitometry (Figure 5(c) and (d)). In addition, correlation analysis of BLI signal (at all time points) with histology (LFB at Day 35) showed statistically significant positive correlations (Figure 5(e)). Among all imaging time points, Day 21 BLI signal and Day 35 LFB data had the strongest correlation (also observed in Supplemental Table 2), which is consistent with the notion that the BLI signal decrease should precede LFB myelin staining measurement.

In addition to histological confirmation of demyelination detected by reduced luciferase signal intensity in MBP-luci mice exposed to cuprizone, the level of myelin loss was measured by MRI in serial coronal sections of the mouse brain, thereby analyzing different regions of the corpus callosum (rostral to caudal). Figure 6(a) shows gray scale MTR images highlighting the corpus callosum as an ROI for measurement and comparison between control diet versus cuprizone diet (4 weeks) using MTR (full color scale, Figure 6(c)) and T2W MRI (Figure 6(e)). The corpus callosum ROI and MRI parameters from the MTR and T2 maps were quantified (Figure 6(b), (d), and (f), respectively). Each data point indicates the average of the measured parameter across all slices in the same animal. The ROI area (Figure 6(b)) and MTR (Figure 6(c) and (d)) showed a significant decrease $(.01 < p < .05)$ in the cuprizone-fed mice compared with the normal diet mice. T2 showed a significant increase $(p < .001)$ in signal (Figure 6(e) and (f)) in the cuprizone-fed mice compared with the normal diet mice. Furthermore, we conducted correlation analysis of BLI data with LFB and MRI parameters (Supplemental Table 2, which shows a separate study than Figure 5). BLI showed a strong correlation with histology LFB staining, corpus callosum area, and T2 MRI signal but not with MTR.

Discussion

This article details the generation, characterization, optimization, and potential application of a new MBP-luci mouse model to test remyelination compounds, where the M1 to M4 promoter regions of the MBP gene drive expression of a luciferase reporter in the CNS. Luciferase activity in the brain was highly correlated with demyelination and remyelination events, as confirmed by both MRI in living mice and postmortem histological analysis with LFB staining of tissue sections. Transgenic mice were used to confirm enhanced remyelination in the cuprizone model after therapeutic treatment with a Sanofi PPAR-δ selective agonist, S711, a small molecule that also stimulated rat OPC differentiation *in vitro* in a concentration dependent manner (Supplemental
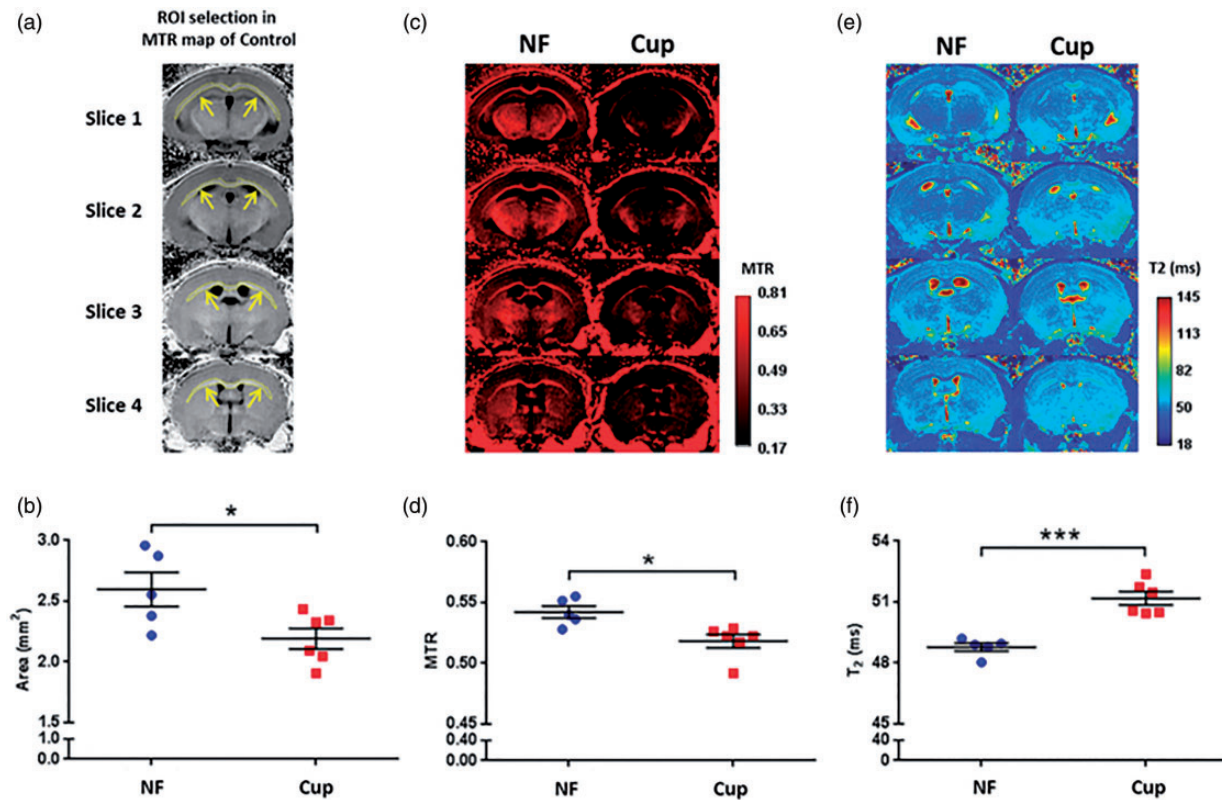
Figure 6. Quantification of myelin changes in the corpus callosum by MRI in a separate study. Only subset of MBP-luci mice were selected for MRI ($n = 5$ for NF and $n = 6$ for Cup). (a) Gray-scale MTR maps from a control mouse are shown across four slices from the direction of the cerebellum toward to the olfactory bulb (Slice 1 to Slice 4 are shown). The outlined yellow region shows the corpus callosum indicated by the arrows. (b) The average area of the corpus callosum across the entire structure in each mouse is shown for each group at the 4-week time point. MTR maps (c) in color scale and MTR quantification (d) are shown for the two groups. T2 maps (e) in color scale and T2 quantification (f) are shown for the two groups. All data are shown at the 4-week time point. Statistically significant differences are indicated on the plots as determined by a two-tailed t test analysis.

Figure 4). Previous reports demonstrate PPAR-δ expression in oligodendrocytes and agonist-driven differentiation *in vitro* (Granneman et al., 1998; Saluja et al., 2001). Importantly, clinical improvement and neuroprotective effects have been linked to PPAR-δ agonist induced effects in a MOG experimental autoimmune encephalomyelitis ($MOG_{35–55}$) model of MS (Polak et al., 2005). In this study, mice were dosed with GW0742 (GlaxoSmithKline) after disease onset, and therapeutic efficacy was linked to both a reduction in astrocytic and microglial inflammatory activation and increased expression of myelin genes in the CNS. The team went on to confirm that the neuroprotective effects were mediated through activation of PPAR-δ and, in oligodendrocytes, may involve modulation of the BMP pathway (Simonini et al., 2010). Together with the S711 findings, this suggests that different PPAR-δ chemical series can stimulate oligodendrocyte differentiation and myelin expression. In addition, MBP-luci mice confirmed a protective effect of QTP, with dosing initiated after 4 weeks of exposure to the cuprizone diet consistent to literature

reports of myelin protection (Bi et al., 2012; Zhang et al., 2012).

Measuring myelin content in the cuprizone model of de/remyelination has been traditionally performed by histological means, utilizing global lipid staining methods including LFB or Black and Gold (Matsushima & Morell, 2001). Alternatively, immunostaining for myelin proteins (MBP, PLP, and MOG) has also been widely reported (Stidworthy et al., 2003; Wergeland et al., 2011). Subsequent digitalization of stained tissue sections and densitometry quantification with specialized software renders a semi-quantitative analysis of demyelination and remyelination. However, analysis of tissue staining for lipid content or immuno-detection of specific myelin proteins as a measure of myelin changes and their consequences in physiology and pathology is known to be highly variable in commonly used models, including the cuprizone model. In addition to strain differences, there are age, sex, and tissue region differences that are both time and labor intensive when assessing by histological means. Moreover, histology requires postmortem

sampling, thereby disqualifying each animal to serve as its own longitudinal control. By contrast, the MBP-luci model allows for the real-time assessment of changes that occur in individual animals during dynamic events, such as myelin loss and repair in the cuprizone model. In depth analysis of the extent of demyelination of cuprizone model at both histological and MBP gene expression level would be ideal for studying the underlying pathophysiological events as well as cellular and molecular changes induced by the loss of myelin.

Identifying reliable biochemical or translational biomarkers for neuroprotective and myelin repair therapies has proven elusive, which has resulted in development and implementation of new imaging technologies as the most suitable methodology to determine myelin content and changes, particularly in the cuprizone model of MS (Silvestroff et al., 2010; Tagge et al., 2016). Imaging measurements of brain volume and myelin content in live rodents present the challenge of low sensitivity to focus on specific brain or spinal cord regions where demyelination might be more pronounced. In this context, creating a reporter gene model suitable for longitudinal analysis of myelin changes in experimental models should provide an invaluable imaging tool for the identification and evaluation of agents capable of enhancing or accelerating myelin repair in drug discovery settings, especially in a high-throughput and noninvasive manner to enable compound screening.

In the initial design of the MBP-luci model and toward the visualization of dynamic myelin changes, we considered a fluorescent MBP model, including the use of green florescent protein; however, the poor signal-to-background ratio due to tissue auto-fluorescence made this less attractive than the bioluminescence-based model. We also considered MRI and other translational imaging modalities; however, the low throughput and lack of cell target specificity was prohibitive. Despite that, a subset of MBP-luci mice were used in MRI validation studies. T2 and MTR values detected cuprizone-induced demyelination effects (Figure 6), which is consistent with published literature (Fjær et al., 2013; Guglielmetti et al., 2016; Tagge et al., 2016). Although T2 showed a strong correlation with the BLI data, MTR did not show the same relationship (Supplemental Table 2). One possible explanation is that our ROI analysis method involved the selection of the entire corpus callosum structure (from the rostral to the caudal sections) while previous studies selected subregions of the corpus callosum (Fjær et al., 2013; Guglielmetti et al., 2016; Tagge et al., 2016). Moreover, the spatial difference of MTR across the corpus callosum has been clearly demonstrated (Tagge et al., 2016), which may have contributed to our limited MTR dynamic window. This disparity may also be related to differences in the mouse strain or background and cuprizone exposure, although larger sample numbers are needed to clarify.

In the neuro-bioimaging field, transgenic reporter gene models allow for the noninvasive visualization and longitudinal evaluation of cellular processes including neurogenesis (DCX-luc, doublecortin promoter-driven luciferase model; Couillard-Despres et al., 2008; Fricke et al., 2017) and astrogliosis (GFP-luc, glial fibrillary acidic protein promoter-driven luciferase model; Zhu et al., 2004; Ho et al., 2007; Biesmans et al., 2015) in live mice (Contag et al., 1998; Contag & Ross, 2002). The MBP-luci model further extends this capacity to monitor myelination events and allows for a combinatorial approach that is expected to further enhance the ability to measure biological changes in real time.

MBP promoter regions have been well characterized using different strategies, including through the random integration of bacterial LacZ gene (Foran & Peterson, 1992; Gow et al., 1992) and the targeted integration into the hypoxanthine-guanine phosphoribosyltransferase locus (Farhadi et al., 2003). The MBP-luci transgenic model was generated through traditional pronuclear injection and as such, the bioluminescence reporters were randomly integrated into the genome. Importantly, several factors can affect transgene expression, including integration locus, copy number, codon usage, mRNA, and protein half-life. However, the expression comparison of endogenous MBP gene and reporter gene lacZ has been analyzed and shown to be well correlated (Gow et al., 1992) and consistent with this finding. The data currently presented suggest that the luciferase reporter gene from MBP-luci mice are similarly well correlated and useful for detecting and tracking dynamic changes in myelin paralleling to endogenous MBP expression (Supplemental Figure 3).

In terms of imaging sensitivity, various luciferase reporter genes have demonstrated superior utility for use in brain imaging, including studying cellular and genetic mechanisms, tracking pathophysiological dynamic process in disease models, and selecting therapeutic candidates (Rettig et al., 2006; Aswendt et al., 2013; Vogel et al., 2017). After the initial characterization and validation of the MBP-luci model (Cao et al., 2011; Cao et al., 2014), we took advantage of both brain and intestinal luciferase expression from line 171 to normalize relative bioluminescence signals and measure intestinal cell apoptosis induced by ionizing radiation with caged luciferin (Cao, Adler, & Ying, 2011). Our efforts to improve model sensitivity included backcrossing the B6C3H mice to the C57BL/6 albino strain and using the newer brain penetrable substrate CycLuc1 (Cao et al., 2016). These efforts resulted in the capacity to image 50 to 100 mice per compound profiling study, thereby improving throughput, which is critical to screening research for drug discovery.

Overall, the primary benefit of the MBP-luci model over other bioimaging solutions is that it enables the visualization of demyelinating and remyelinating events in live mice noninvasively, over time with each animal serving as its own control and with extremely high signal-to-background ratio for semiquantitative analysis. This allows for ongoing assessment of therapeutic effects and biological variability including age, sex, and disease states. This longitudinal tool is anticipated to significantly reduce the resource and manpower demands associated with labor intensive chronic animal studies and postmortem histochemical or gene expression analyses and provide a sensitive *in vivo* approach for targeting and therapeutic validation and prioritization.

Author Contributions

J. C. designed and constructed MBP-luci vectors, carried out all validation and compound profiling studies, and performed model optimization and data analysis; Y. H. set up the cuprizone model and directed animal breeding for studies at the Framingham site and edited the manuscript; M. S. S. conducted the MRI studies, data analysis, and edited the manuscript; N. P. and D. W. provided histology and analysis support at the Framingham and Bridgewater sites, respectively. G. H. P. led transgenic model generation and provided critical feedback to studies at Bridgewater site; C. P. directs model application at Framingham site. K. J. C. initiated and co-led model development, provided scientific guidance for cuprizone studies, and directed the PPAR-δ studies at the formal Bridgewater research site; W. Z. guided the statistical analysis and statistical question answers from reviewers. X. Y. initiated imaging model design and co-led model development, initiated *in vivo* imaging and performed in situ or ex vivo imaging validation studies, and edited the manuscript. J. C., K. J. C., and C. P. drafted or edited the manuscript. All studies were conducted in Sanofi's Research Sites. All authors approved the final version of the manuscript.

Declaration of Conflicting Interests

The author(s) declared the following potential conflicts of interest with respect to the research, authorship, and/or publication of this article: All authors are/were Sanofi employees during this research.

References

Adams, C. W. M. (1989). *A color atlas of multiple sclerosis & other myelin disorders*. London, England: Wolfe Medical Publications.

Adams, S. T., Jr., & Miller, S. C. (2014). Beyond D-luciferin: Expanding the scope of bioluminescence imaging in vivo. *Curr Opin Chem Biol*, *21*, 112–120.

Aswendt, M., Adamczak, J., Couillard-Despres, S., & Hoehn, M. (2013). Boosting bioluminescence neuroimaging: An optimized protocol for brain studies. *PLoS One*, *8*, e55662.

Barres, B. A., & Raff, M. C. (1999). Axonal control of oligodendrocyte development. *J Cell Biol*, *147*, 1123–1128.

Berger, F., Paulmurugan, R., Bhaumik, S., & Gambhir, S. S. (2008). Uptake kinetics and biodistribution of 14C-D-luciferin—A radiolabeled substrate for the firefly luciferase catalyzed bioluminescence reaction: Impact on bioluminescence based reporter gene imaging. *Eur J Nucl Med Mol Imaging*, *35*, 2275–2285.

Bi, X., Zhang, Y., Yan, B., Fang, S., He, J., Zhang, D., Zhang, Z., Kong, J., Tan, Q., & Li, X. M. (2012). Quetiapine prevents oligodendrocyte and myelin loss and promotes maturation of oligodendrocyte progenitors in the hippocampus of global cerebral ischemia mice. *J Neurochem*, *123*, 14–20.

Biesmans, S., Acton, P. D., Cotto, C., Langlois, X., Ver Donck, L., Bouwknecht, J. A., Aelvoet, S. A., Hellings, N., Meert, T. F., & Nuydens, R. (2015). Effect of stress and peripheral immune activation on astrocyte activation in transgenic bioluminescent Gfap-luc mice. *Glia*, *63*, 1126–1137.

Cao, J., Adler, D., & Ying, X. (2011). High-sensitive in vivo photonic imaging of apoptotic cells by utilizing transgenic mouse models. In NYAS editorial staff (eds) *Animal models and their value in predicting drug efficacy and toxicity* (p. 96). New York City, NY: New York Academy Science.

Cao, J., Chandross, K., Economides, K. D., Polites, H. G., Weinstock, D., & Ying, X. (2011). *Animal model expressing luciferase under control of the myelin basic protein promoter (mbp-luci) and use of the model for bioluminescence in vivo imaging*. Patent number WO/2011/084281.

Cao, J., Hu, Y., Siders, B., Chandross, K., Ruble, G., & Ying, X. (2014). A transgenic mouse model with the myelin basic protein promoter controlled luciferase reporter. In ■ *World molecular imaging society* annual meeting proceedings (p. P581). Seoul, South Korea.

Cao, J., Hu, Y., Siders, B., & Ying, X. (2016). Using of optical imaging to measure BBB permeability in live mice. In ■ *World molecular imaging society* annual meeting proceedings (p. P482). New York City, NY.

Chang, A., Nishiyama, A., Peterson, J., Prineas, J., & Trapp, B. D. (2000). NG2-positive oligodendrocyte progenitor cells in adult human brain and multiple sclerosis lesions. *J Neurosci*, 20, 6404–6412.

Contag, C. H., & Ross, B. D. (2002). It's not just about anatomy: In vivo bioluminescence imaging as an eyepiece into biology. *J Magn Reson Imaging*, 16, 378–387.

Contag, P. R., Olomu, I. N., Stevenson, D. K., & Contag, C. H. (1998). Bioluminescent indicators in living mammals. *Nat Med*, 4, 245–247.

Corboy, J. R., & Miravalle, A. A. (2010). Emerging therapies for treatment of multiple sclerosis. *J Inflamm Res*, 3, 53–59.

Couillard-Despres, S., Finkl, R., Winner, B., Ploetz, S., Wiedermann, D., Aigner, R., Bogdahn, U., Winkler, J., Hoehn, M., & Aigner, L. (2008). In vivo optical imaging of neurogenesis: Watching new neurons in the intact brain. *Mol Imaging*, 7, 28–34.

Decker, L., Picard, N., Lachapelle, F., & Baron-Van Evercooren, A. (2001). Neural precursors and demyelinating diseases. *Prog Brain Res*, 132, 175–184.

Elsworth, S., & Howell, J. M. (1973). Variation in the response of mice to cuprizone. *Res Vet Sci*, 14, 385–387.

Evans, M. S., Chaurette, J. P., Adams, S. T., Jr., Reddy, G. R., Paley, M. A., Aronin, N., Prescher, J. A., & Miller, S. C. (2014). A synthetic luciferin improves bioluminescence imaging in live mice. *Nat Methods*, 11, 393–395.

Farhadi, H. F., Lepage, P., Forghani, R., Friedman, H. C., Orfali, W., Jasmin, L., Miller, W., Hudson, T. J., & Peterson, A. C. (2003). A combinatorial network of evolutionarily conserved myelin basic protein regulatory sequences confers distinct glial-specific phenotypes. *J Neurosci*, 23, 10214–10223.

Fjær, S., Bø, L., Lundervold, A., Myhr, K. M., Pavlin, T., Torkildsen, O., & Wergeland, S. (2013). Deep gray matter demyelination detected by magnetization transfer ratio in the cuprizone model. *PLoS One*, 8, e84162.

Foran, D. R., & Peterson, A. C. (1992). Myelin acquisition in the central nervous system of the mouse revealed by an MBP-Lac Z transgene. *J Neurosci*, 12, 4890–4897.

Fricke, I. B., Schelhaas, S., Zinnhardt, B., Viel, T., Hermann, S., Couillard-Despres, S., & Jacobs, A. H. (2017). In vivo bioluminescence imaging of neurogenesis—The role of the blood brain barrier in an experimental model of Parkinson's disease. *Eur J Neurosci*, 45, 975–986.

Gow, A., Friedrich, V. L., Jr., & Lazzarini, R. A. (1992). Myelin basic protein gene contains separate enhancers for oligodendrocyte and Schwann cell expression. *J Cell Biol*, 119, 605–616.

Grade, S., Bernardino, L., & Malva, J. O. (2013). Oligodendrogenesis from neural stem cells: Perspectives for remyelinating strategies. *Int J Dev Neurosci*, 31, 692–700.

Granneman, J., Skoff, R., & Yang, X. (1998). Member of the peroxisome proliferator-activated receptor family of transcription factors is differentially expressed by oligodendrocytes. *J Neurosci Res*, 51, 563–573.

Guglielmetti, C., Le Blon, D., Santermans, E., Salas-Perdomo, A., Daans, J., De Vocht, N., Shah, D., Hoornaert, C., Praet, J., Peerlings, J., Kara, F., Bigot, C., Mai, Z., Goossens, H., Hens, N., Hendrix, S., Verhoye, M., Planas, A. M., Berneman, Z., van der Linden, A., & Ponsaerts, P. (2016). Interleukin-13 immune gene therapy prevents CNS inflammation and demyelination via alternative activation of microglia and macrophages. *Glia*, 64, 2181–2200.

Ho, G., Zhang, C., & Zhuo, L. (2007). Non-invasive fluorescent imaging of gliosis in transgenic mice for profiling developmental neurotoxicity. *Toxicol Appl Pharmacol*, 221, 76–85.

Iwashita, A., Muramatsu, Y., Yamazaki, T., Muramoto, M., Kita, Y., Yamazaki, S., Mihara, K., Moriguchi, A., & Matsuoka, N. (2007). Neuroprotective efficacy of the peroxisome proliferator-activated receptor delta-selective agonists in vitro and in vivo. *J Pharmacol Exp Ther*, 320, 1087–1096.

Jurevics, H., Largent, C., Hostettler, J., Sammond, D. W., Matsushima, G. K., Kleindienst, A., Toews, A. D., & Morell, P. (2002). Alterations in metabolism and gene expression in brain regions during cuprizone-induced demyelination and remyelination. *J Neurochem*, 82, 126–136.

Lindner, M., Heine, S., Haastert, K., Garde, N., Fokuhl, J., Linsmeier, F., Grothe, C., Baumgärtner, W., & Stangel, M. (2008). Sequential myelin protein expression during remyelination reveals fast and efficient repair after central nervous system demyelination. *Neuropathol Appl Neurobiol*, 34, 105–114.

Lee, K. H., Byun, S. S., Paik, J. Y., Lee, S. Y., Song, S. H., Choe, Y. S., & Kim, B. T. (2003). Cell uptake and tissue distribution of radioiodine labelled D-luciferin: Implications for luciferase based gene imaging. *Nucl Med Commun*, 24, 1003–1009.

Mangiardi, M., Crawford, D. K., Xia, X., Du, S., Simon-Freeman, R., Voskuhl, R. R., & Tiwari-Woodruff, S. K. (2011). An animal model of cortical and callosal pathology in multiple sclerosis. *Brain Pathol*, 21, 263–278.

Matsushima, G. K., & Morell, P. (2001). The neurotoxicant, cuprizone, as a model to study demyelination and remyelination in the central nervous system. *Brain Pathol*, 11, 107–116.

Miron, V. E., Kuhlmann, T., & Antel, J. P. (2011). Cells of the oligodendroglial lineage, myelination, and remyelination. *Biochim Biophys Acta*, 1812, 184–193.

Nakahara, J., Aiso, S., & Suzuki, N. (2009). Factors that retard remyelination in multiple sclerosis with a focus on TIP30: A novel therapeutic target. *Expert Opin Ther Targets*, 13, 1375–1386.

Piaton, G., Williams, A., Seilhean, D., & Lubetzki, C. (2009). Remyelination in multiple sclerosis. *Prog Brain Res*, 175, 453–464.

Plemel, J. R., Liu, W. Q., & Yong, V. W. (2017). Remyelination therapies: A new direction and challenge in multiple sclerosis. *Nat Rev Drug Discov*, 16, 617–634.

Polak, P. E., Kalinin, S., Dello Russo, C., Gavrilyuk, V., Sharp, A., Peters, J. M., Richardson, J., Willson, T. M., Weinberg,

G., & Feinstein, D. L. (2005). Protective effects of a perox-isome proliferator-activated receptor-beta/delta agonist in experimental autoimmune encephalomyelitis. *J Neuroimmunol*, *168*, 65–75.

Polites, H. G., & Pinkert, C. A. (2002). CHAPTER 2—DNA microinjection and transgenic animal production. In Carl Pinkert (Ed.), *Transgenic animal technology* (2nd ed., pp. 15–70). San Diego, CA: Academic Press.

Raff, M. C., & Lillien, L. E. (1988). Differentiation of a bipo-tential glial progenitor cell: What controls the timing and the choice of developmental pathway? *J Cell Sci Suppl*, *10*, 77–83.

Rettig, G. R., McAnuff, M., Liu, D., Kim, J. S., & Rice, K. G. (2006). Quantitative bioluminescence imaging of transgene expression in vivo. *Anal Biochem*, *355*, 90–94.

Saluja, I., Granneman, J. G., & Skoff, R. P. (2001). PPAR delta agonists stimulate oligodendrocyte differentiation in tissue culture. *Glia*, *33*, 191–204.

Silvestroff, L., Bartucci, S., Soto, E., Gallo, V., Pasquini, J., & Franco, P. (2010). Cuprizone-induced demyelination in CNP::GFP transgenic mice. *J Comp Neurol*, *518*, 2261–2283.

Simonini, M., Polak, P. E., Boullerne, A. I., Peters, J. M., Richardson, J. C., & Feinstein, D. L. (2010). Regulation of oligodendrocyte progenitor cell maturation by PPARd: Effects on bone morphogenetic proteins. *ASN Neuro*, *2*, e00025.

Stidworthy, M. F., Genoud, S., Suter, U., Mantei, N., & Franklin, R. J. (2003). Quantifying the early stages of remyelination following cuprizone-induced demyelination. *Brain Pathol*, *13*, 329–339.

Tagge, I., O'Connor, A., Chaudhary, P., Pollaro, J., Berlow, Y., Chalupsky, M., Bourdette, D., Woltjer, R., Johnson, M., & Rooney, W. (2016). Spatio-temporal patterns of demyelin-ation and remyelination in the cuprizone mouse model. *PLoS One*, *11*, e0152480.

Vogel, S., Collmann, F. M., & Hoehn, M. (2017). Perspectives of in vivo bioluminescence imaging: Application to basic and translational neuroscience. *Curr Pharm Des*, *23*, 1963–1973.

Wergeland, S., Torkildsen, O., Myhr, K. M., Aksnes, L., Mork, S. J., & Bo, L. (2011). Dietary vitamin D3 supplements reduce demyelination in the cuprizone model. *PLoS One*, *6*, e26262.

Yu, Q., Hui, R., Park, J., Huang, Y., Kusnecov, A. W., Dreyfus, C. F., & Zhou, R. (2017). Strain differences in cuprizone induced demyelination. *Cell Biosci*, *7*, 59.

Zhang, Y., Zhang, H., Wang, L., Jiang, W., Xu, H., Xiao, L., Bi, X., Wang, J., Zhu, S., Zhang, R., He, J., Tan, Q., Zhang, D., Kong, J., & Li, X. M. (2012). Quetiapine enhances oli-godendrocyte regeneration and myelin repair after cuprizone-induced demyelination. *Schizophr Res*, *138*, 8–17.

Zhu, L., Ramboz, S., Hewitt, D., Boring, L., Grass, D. S., & Purchio, A. F. (2004). Non-invasive imaging of GFAP expression after neuronal damage in mice. *Neurosci Lett*, *367*, 210–212.